Performance Evaluation of Nondegenerate Wavelength Conversion in a Silicon Nanowire Waveguide

Shiming Gao, *Member, IEEE, OSA*, Zhiqiang Li, En-Kuang Tien, *Student Member, IEEE, OSA*, Sailing He, *Senior Member, IEEE, Fellow, OSA*, and Ozdal Boyraz, *Member, IEEE*

***Abstract*—The performance of wavelength conversion based on nondegenerate four-wave mixing (FWM) with two pumps is theoretically evaluated in a silicon nanowire waveguide. A theoretical model is developed to take into the limitations of nonlinear loss parameters on conversion bandwidth, efficiency, and uniformity. Analysis shows that the conversion bandwidth of two-pump nondegenerate FWM is $>30\%$ broader than the conversion bandwidth of the degenerate FWM without compromising the conversion efficiency under the same pump power level. Also the results indicate that the improvement originates from efficient phase matching over broader bandwidth range due to two-wavelength pumps.**

***Index Terms*—Nonlinear optics, optical frequency conversion, optical mixing, optical planar waveguides, silicon on insulator technology.**

I. Introduction

In recent years, nonlinear effects in silicon nanowire waveguides have been considered as the promising solution for high-density integrated signal processing components [1], [2]. In particular, four-wave mixing (FWM) in silicon waveguides has been used to realize optical sampling [3], parametric amplification [4], [5], optical regeneration [6], and wavelength conversion [7]–[13] for the next generation high-speed optical communication systems. However, to achieve a viable solution for real-life optical communication applications via FWM and to minimize the detrimental effects of nonlinear absorptions, high conversion efficiency and broad conversion bandwidth are two critical parameters which need to be optimized [5]. Many efforts have been made to improve the conversion efficiency and conversion bandwidth such as utilizing micro-ring resonators [13] and optimizing the pump parameters and the waveguide geometries through dispersion engineering in conventional waveguides [14]–[16] or in a design of multi-layer structure [17]. Impediments due to the polarization dependency of FWM have also been studied and practical solutions for real-life applications have been proposed [18]. Most of these investigations were based on the single-pump degenerate FWM. The nondegenerate FWM using two pumps has also been mentioned in several references. For example, the two-pump FWM was used to flatten the conversion response in the pulse-pumped regime without free-carrier absorption considered [15]. Multiple idlers around the signal were generated by using a multi-longitudinal-mode pump [11]. Broadband one-to-two wavelength conversion was realized by setting one pump near the signal and scanning the other pump [19]. Also, ten mixing sidebands were obtained by injecting two pumps and a signal into the silicon waveguide in a similar setup [20].

In principle, the use of single pump in silicon waveguides comes with rigid phase matching since the dominated factors, both the pump wave number and the pump power, are hard to be tuned due to the inherent principle of single-pump FWM and the nonlinear losses through two-photon absorption (TPA) and free-carrier absorption (FCA). However, the nondegenerate FWM process based on two pumps shows more flexibility to achieve the phase matching. If nondegenerate FWM with two pumps is used for wavelength conversion, the signals around each pump have small phase mismatches wherever the pumps are set. Hence, the phase-matching map can be easily tuned by changing the setting of the pump wavelengths. Since the conversion bandwidth is tightly controlled by the phase-matching condition, it can also be efficiently enhanced by optimizing the incident pumps.

In this paper, we investigate the wavelength conversion scheme based on nondegenerate FWM in silicon nanowire waveguides with two incident pumps in terms of conversion bandwidth and efficiency through the comparison with the traditional degenerate FWM. In particular, the influences of TPA and FCA are taken into account since they are significant under the quasi-continuous wave assumption even though it may be neglected in the ultra-short pulse regime [15]. It is predicted that the bandwidth of the nondegenerate FWM-based wavelength conversion is $>30\%$ broader than that of the degenerate FWM under the same efficiency level. The efficiency degrades rapidly

Manuscript received July 07, 2010; accepted September 04, 2010. Date of publication September 13, 2010; date of current version October 20, 2010. This work was supported in part by the National Natural Science Foundation of China under Grant 60708006 and Grant 60978026, in part by the Specialized Research Fund for the Doctoral Program of Higher Education of China under Grant 20070335118, in part by the Zhejiang Provincial Natural Science Foundation of China under Grant Y1090379, and in part by the DARPA Young Faculty Award under Grant N66001-10-1-4036.

S. Gao is with the Centre for Optical and Electromagnetic Research, State Key Laboratory of Modern Optical Instrumentation, Zhejiang University, Hangzhou 310058, China. He is also with the Department of Electrical Engineering and Computer Science, University of California, Irvine, CA 92697 USA (e-mail: gaosm@zju.edu.cn).

Z. Li and S. He are with the Centre for Optical and Electromagnetic Research, State Key Laboratory of Modern Optical Instrumentation, Zhejiang University, Hangzhou 310058, China.

E.-K. Tien is with the Department of Electrical Engineering and Computer Science, University of California, Irvine, CA 92697 USA.

O. Boyraz is with the Department of Electrical Engineering and Computer Science, University of California, Irvine, CA 92697 USA. He is also with the Department of Electrical and Electronics Engineering, Istanbul Sehir University, Istanbul 34662, Turkey.

Digital Object Identifier 10.1109/JLT.2010.2076333

with increasing free carrier lifetime. Also, the FCA limitation is found to be almost the same as the degenerate FWM process.

II. Theoretical Analysis

In the nondegenerate FWM, two pump waves (λ_{p1} and λ_{p2}) are used. Assuming both of the pumps are co-polarized as the TE axis, they interact with the TE-polarized signal wave at λ_s in the silicon nanowire waveguide and a converted wave at $\lambda_c = 1/(1/\lambda_{p1} + 1/\lambda_{p2} - 1/\lambda_s)$ will be generated, as shown in Fig. 1. Considering the linear loss, the TPA- and FCA-induced nonlinear losses, self-phase modulation (SPM), and cross-phase modulation (XPM), the coupled equations for this FWM process under the quasi-continuous wave assumption can be expressed as [1], [16]

$$\begin{aligned}\frac{dA_{p1}}{dz} &= -\frac{1}{2}(\alpha_{p1}+\alpha_{\mathrm{TPA}p1}+\alpha_{\mathrm{FCA}p1})A_{p1} \\ &\quad + j\gamma_{p1}[|A_{p1}|^2+2|A_{p2}|^2+2|A_s|^2+2|A_c|^2]A_{p1} \\ &\quad + 2j\gamma_{p1}A_{p2}^*A_sA_c\exp(j\Delta\beta z) \quad (1)\\ \frac{dA_{p2}}{dz} &= -\frac{1}{2}(\alpha_{p2}+\alpha_{\mathrm{TPA}p2}+\alpha_{\mathrm{FCA}p2})A_{p2} \\ &\quad + j\gamma_{p2}[2|A_{p1}|^2+|A_{p2}|^2+2|A_s|^2+2|A_c|^2]A_{p2} \\ &\quad + 2j\gamma_{p2}A_{p1}^*A_sA_c\exp(j\Delta\beta z) \quad (2)\\ \frac{dA_s}{dz} &= -\frac{1}{2}(\alpha_s+\alpha_{\mathrm{TPAs}}+\alpha_{\mathrm{FCAs}})A_s \\ &\quad + j\gamma_s[2|A_{p1}|^2+2|A_{p2}|^2+|A_s|^2+2|A_c|^2]A_s \\ &\quad + 2j\gamma_sA_c^*A_{p1}A_{p2}\exp(-j\Delta\beta z) \quad (3)\\ \frac{dA_c}{dz} &= -\frac{1}{2}(\alpha_c+\alpha_{\mathrm{TPAc}}+\alpha_{\mathrm{FCAc}})A_c \\ &\quad + j\gamma_c[2|A_{p1}|^2+2|A_{p2}|^2+2|A_s|^2+|A_c|^2]A_c \\ &\quad + 2j\gamma_cA_s^*A_{p1}A_{p2}\exp(-j\Delta\beta z) \quad (4)\end{aligned}$$

where $A_{p1,p2,s,c}(z)$ are the amplitudes of the pump, signal and converted waves, $\gamma_{p1,p2,s,c}$ are the nonlinear coefficients, $\Delta\beta$ is the linear phase mismatch, $\alpha_{p1,p2,s,c}$ are the linear-loss coefficients, $\alpha_{\mathrm{TPA}p1,p2,s,c}$ and $\alpha_{\mathrm{FCA}p1,p2,s,c}$ are the nonlinear-loss coefficients caused by the TPA and FCA effects. In semiconductors, the main nonlinear losses originate from TPA and TPA-induced FCA at operation wavelengths where photon energy is $E_g/2 < h\nu < E_g$. Mathematically the loss coefficient induced by TPA can be expressed as [21]

$$\alpha_{\mathrm{TPA}i} = \frac{\beta_{\mathrm{TPA}}}{A_{\mathrm{eff}}}\left(|A_i|^2 + 2\sum_{m\neq i}|A_m|^2\right) \quad (i=p1,p2,s,c;\, m=p1,p2,s,c). \quad (5)$$

where β_{TPA} is the TPA coefficient and A_{eff} is the effective mode area.

According to (5), the optical powers absorbed due to the degenerate and nondegenerate TPAs along the waveguide may be described as [22]

$$P_{\mathrm{TPA}m}(z) = \frac{\beta_{\mathrm{TPA}}}{A_{\mathrm{eff}}}|A_m|^4, \quad (m=p1,p2,s,c) \quad (6)$$

$$P_{\mathrm{TPA}mn}(z) = \frac{2\beta_{\mathrm{TPA}}}{A_{\mathrm{eff}}}|A_m|^2|A_n|^2, \quad (m=p1,p2,s,c;\, n=p1,p2,s,c). \quad (7)$$

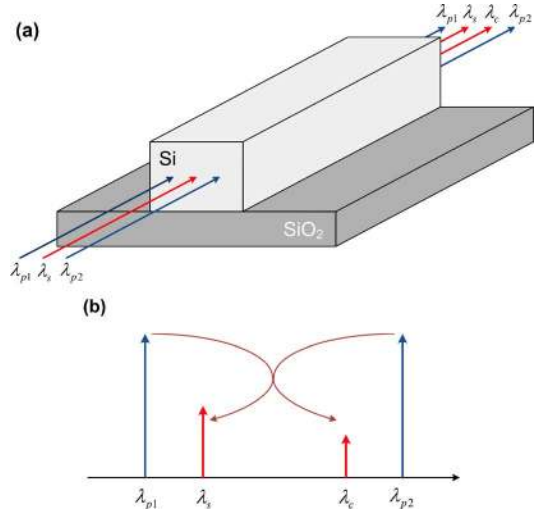

Fig. 1. Schematic description of the wavelength conversion based on nondegenerate FWM with two pumps.

A pair of free carriers will be generated for every two photons being absorbed. The rate of free-carrier generation and recombination inside the waveguide is described using the following equation by simultaneously considering the degenerate and nondegenerate TPAs

$$\frac{dN}{dt} = \sum_m \frac{P_{\mathrm{TPA}m}}{2h\nu_m} + \sum_{m\neq n}\frac{P_{\mathrm{TPA}mn}}{h\nu_m + h\nu_n} - \frac{N}{\tau}, \quad (m=p1,p2,s,c;\, n=p1,p2,s,c) \quad (8)$$

where $\nu_{p1,p2,s,c}$ are the frequency of the interacting waves, τ is the effective free-carrier lifetime, h is the Planck's constant.

At steady state, i.e., $dN/dt = 0$, the free-carrier density can be expressed as [23]

$$N(z) = \frac{\beta_{\mathrm{TPA}}\tau}{A_{\mathrm{eff}}}\left(\sum_m \frac{|A_m|^4}{2h\nu_m} + 2\sum_{m\neq n}\frac{|A_m|^2|A_n|^2}{h\nu_m + h\nu_n}\right), \quad (m=p1,p2,s,c;\, n=p1,p2,s,c) \quad (9)$$

And then, the FCA loss coefficient can be calculated using (9) and $\nu_{p1,p2,s,c} = c/\lambda_{p1,p2,s,c}$:

$$\begin{aligned}&\alpha_{\mathrm{FCA}i} \\ &= \sigma_i N = \frac{\sigma_i\beta_{\mathrm{TPA}}\tau}{2hcA_{\mathrm{eff}}^2} \\ &\quad\times\left(\sum_m \lambda_m|A_m|^4 + 4\sum_{m\neq n}\frac{\lambda_m\lambda_n|A_m|^2|A_n|^2}{\lambda_m+\lambda_n}\right) \\ &(i=p1,p2,s,c;\, m=p1,p2,s,c;\, n=p1,p2,s,c) \quad (10)\end{aligned}$$

where $\sigma_{p1,p2,s,c}$ are the FCA cross sections.

Denoting the nonlinear index coefficient of silicon as n_2, the nonlinear coefficients for the involved waves can be calculated as

$$\gamma_i = 2\pi n_2/\lambda_i A_{\mathrm{eff}}, \quad (i=p1,p2,s,c) \quad (11)$$

The linear phase mismatch is a factor depends on the different wave numbers of the interacting waves and it is expressed as

$$\begin{aligned}\Delta\beta &= \beta_s + \beta_c - \beta_{p1} - \beta_{p2} \\ &= 2\pi(n_s/\lambda_s + n_c/\lambda_c - n_{p1}/\lambda_{p1} - n_{p2}/\lambda_{p2}) \quad (12)\end{aligned}$$

where $\beta_{p1,p2,s,c}$ are the wave numbers of the interacting waves, which can be calculated by the corresponding effective refractive indexes $n_{p1,p2,s,c}$ in the silicon nanowire waveguide.

Since all the involved waves are in the same wavelength region, it is reasonable to consider the linear-loss coefficients $\alpha_{p1} = \alpha_{p2} = \alpha_s = \alpha_c = \alpha$, and the FCA cross sections $\sigma_{p1} = \sigma_{p2} = \sigma_s = \sigma_c = \sigma$. Because SPM and XPM introduce an additional phase shift to the FWM process, the phase mismatch is also a function of the interacting wave powers besides the involved wavelength numbers. Supposing $P_{p1,p2,s,c} = |A_{p1,p2,s,c}|^2$ and $\gamma_{p1} = \gamma_{p2} = \gamma_s = \gamma_c = \gamma$, and ignoring the phase shift due to the signal and converted waves, the total phase mismatch can be reduced to a simple expression

$$\kappa = \Delta\beta + \gamma(P_{p1} + P_{p2}). \quad (13)$$

In the nondegenerate FWM with two pumps, the linear phase mismatch $\Delta\beta$ can be freely tuned by the two pump wavelengths, which provides the possibility of bandwidth enhancement. Under lossy cases and saturation regimes only numerical solutions are available for the coupled equations (1)–(4). They can be numerically solved using the common Euler method or Runge–Kutta method. In particular the solution to (4) leads to the definition of the conversion efficiency and the conversion bandwidth. The calculation of conversion efficiency, which is defined as

$$\eta(\text{dB}) = 10\log_{10}[P_c(z)/P_s(0)] \quad (14)$$

provides an easy solution to the determination of the conversion bandwidth after solving (1)–(4) numerically.

III. Conversion Bandwidth

The conversion bandwidth is one of the important figures of merit of FWM-based wavelength converters. In this section, the bandwidth performance of the wavelength conversion based on the nondegenerate FWM is analyzed in comparison with the degenerate FWM. Preliminary calculations are performed in a 1.5-cm-long 300 nm × 650 nm (Height × Width) silicon nanowire waveguide that corresponds to 0.12158 μm^2 effective mode area. Fig. 2 shows the TE-polarized effective refractive index and the corresponding dispersion calculated via beam propagation method, where the steps for the cross section and propagating directions are set to be 10 nm and 1 nm, respectively. It is shown that the zero-dispersion wavelength is at 1456 nm. Such dispersion profile is suitable to be used for telecommunication-band wavelength conversion.

For the degenerate FWM-based wavelength conversion, the phase mismatch can be written as $\kappa' = \Delta\beta + 2\gamma P_p$, where P_p represents the pump power [24]. Since the pump power attenuates along the propagation length, the phase mismatch will vary with respect to the distance even though the signal wavelength is fixed

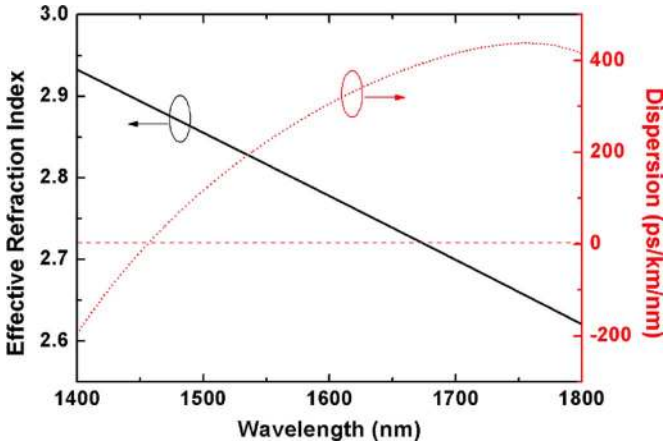

Fig. 2. TE-polarized effective refractive index and the corresponding dispersion as the wavelength varies in a 300 nm × 650 nm silicon nanowire waveguide.

[16], [25]. Figs. 3(a) and (b) simulate the phase mismatches for the pump powers of 100 mW and 1000 mW in the above waveguide and the pump wave is assumed at 1550 nm. In our calculation, the linear propagation loss coefficient is assumed to be $\alpha = 2.5$ dB/cm, the TPA coefficient is $\beta_{\text{TPA}} = 0.8$ cm/GW for both degenerate and nondegenerate absorptions, the FCA cross section is $\sigma = 1.45 \times 10^{-17}$ cm^2, the effective free-carrier lifetime of carriers is $\tau = 2$ ns, and the nonlinear index coefficient is $n_2 = 9\times10^{-18}$ m^2/W. One can see that the exact phase-matching curves in Figs. 3(a) and (b) are quite similar particularly after propagating 0.5 cm in the silicon waveguide, although the incident pump powers are dramatically different. This effect results in the nonlinear loss due to TPA and FCA, especially where FCA is quadratically proportional to the pump powers. A high incident power will be attenuated rapidly to a relatively low level. As a result, the phase mismatch is slightly changed by the pump power. Fig. 4 shows the conversion responses for the two cases corresponding to Fig. 3 with a signal power of 1 mW. The 3-dB conversion bandwidths are 71.5 and 77.2 nm when 100-mW and 1000-mW pumps are adopted. The bandwidth enhancement is very limited by changing the pump power.

In contrast, the phase mismatch can be greatly changed by setting the two pump wavelengths in the nondegenerate FWM scheme. When the mean pump wavelength is fixed at 1550 nm, the phase mismatch is calculated by using (13) with pump spacing of 0 and 61.56 nm, as shown in Figs. 5(a) and (b), in which the pump powers are fixed at 100 mW. According to (12), the linear phase mismatch $\Delta\beta$ is directly determined by the pump wave numbers, that is, the pump wavelengths. In Fig. 5, one can find that the total phase mismatch is sensitive to the pump wavelength spacing and the perfect phase-matching curves $(\kappa = 0)$ separate from each other in the contour map with the pump spacing increasing, which means the enhancement of bandwidth. The simulation results of the conversion responses are shown in Fig. 6. The 3-dB bandwidth is 70.4 nm when the two pumps are very close, which is quite similar to the degenerate FWM. When the two pumps go away from each other, the bandwidth is enhanced gradually. For the pump wavelength spacing of 61.56 nm, the bandwidth reaches 93.3

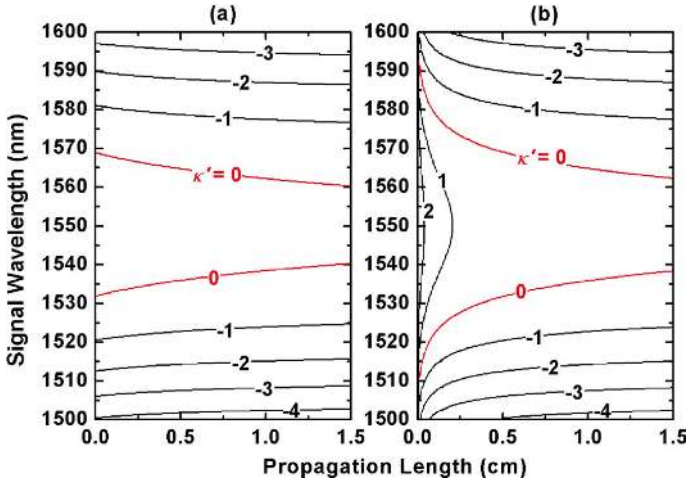

Fig. 3. Phase mismatch (in the units of cm^{-1}) of the degenerate FWM as a function of the signal wavelength and the propagation length with the pump power of (a) 100 mW or (b) 1000 mW.

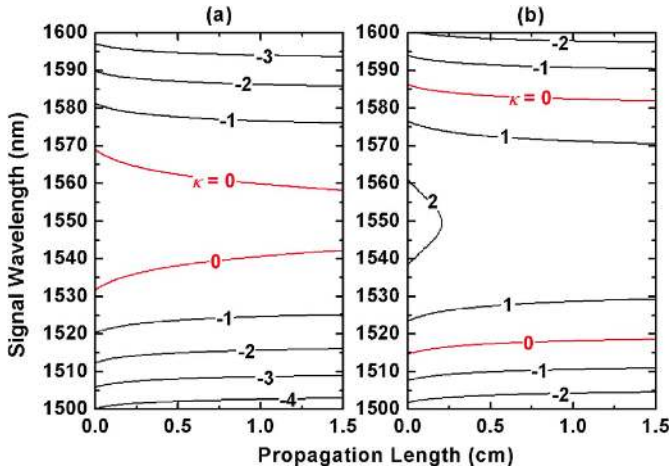

Fig. 5. Phase mismatch (in the units of cm^{-1}) of the nondegenerate FWM as a function of the signal wavelength and the propagation length when the wavelength spacing between the two pumps is (a) 0 and (b) 61.56 nm. Here both pumps have a power of 100 mW and the mean wavelength is 1550 nm.

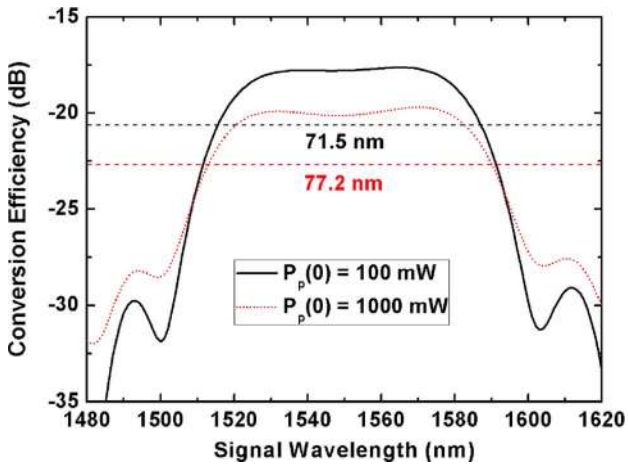

Fig. 4. Degenerate conversion efficiency as the signal wavelength for the pump power of 100 mW or 1000 mW.

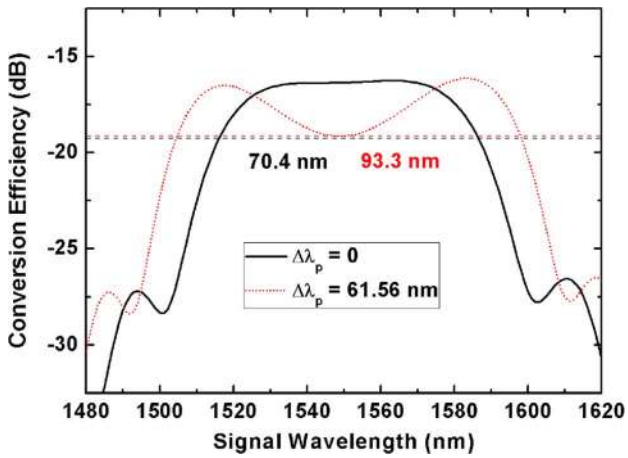

Fig. 6. Nondegenerate conversion efficiency as the signal wavelength varies. Here the wavelength spacing between the two pumps is 0 or 61.56 nm with the same pump condition as Fig. 5.

nm, which is enhanced by 22.9 nm (33%) compared with the case the two pumps are put closely.

The nonuniformity of the conversion response is also concomitantly enhanced with the pump spacing of the nondegenerate FWM increasing since the central signals suffer from larger phase mismatch, which means lower conversion efficiency. For convenience, we define the efficiency difference between the maximum efficiency and the central minimum efficiency as the response nonuniformity. Fig. 7 shows the response variation with the pump power of the degenerate FWM [Fig. 7(a)] or the pump wavelength spacing of the nondegenerate FWM [Fig. 7(b)]. In Fig. 7(b), one can see that the response nonuniformity is also enhanced together with the conversion bandwidth by separating the two pumps. The response nonuniformity reaches 3 dB for 61.56-nm wavelength spacing. Further increasing the pump spacing results in a response nonuniformity of more than 3 dB and the 3-dB bandwidth is divided into two regions, as illustrated in Fig. 7(b). Also, the conversion bandwidth will decrease as the pump spacing increases, which is not beneficial to the wavelength conversion function. With both pump powers of 100 mW, the conversion bandwidth and the corresponding response nonuniformity are quantitatively simulated versus the pump wavelength spacing, as shown in Fig. 8. The maximum 3-dB bandwidth of 93.3 nm can be achieved just when the response nonuniformity is 3 dB.

IV. Conversion Efficiency

For a wavelength conversion scheme, the conversion efficiency is another important parameter which needs to be analyzed under various constraints. In the quasi-continuous wave regime, the FCA will be the dominate loss in the silicon waveguide, which greatly affects the conversion efficiency. Fig. 9 shows the calculated maximum efficiencies for the cases with and without FCA in the two-pump FWM as the pump powers vary, where both of the pump powers are assumed to be equal, and the pump spacing is 50 nm with a mean wavelength at 1550 nm. The inset shows the conversion responses when both of the pump powers are assumed to be 150 mW. One can see that the efficiency discrepancy is very large and even more than 15 dB when the FCA loss is taken into account or not.

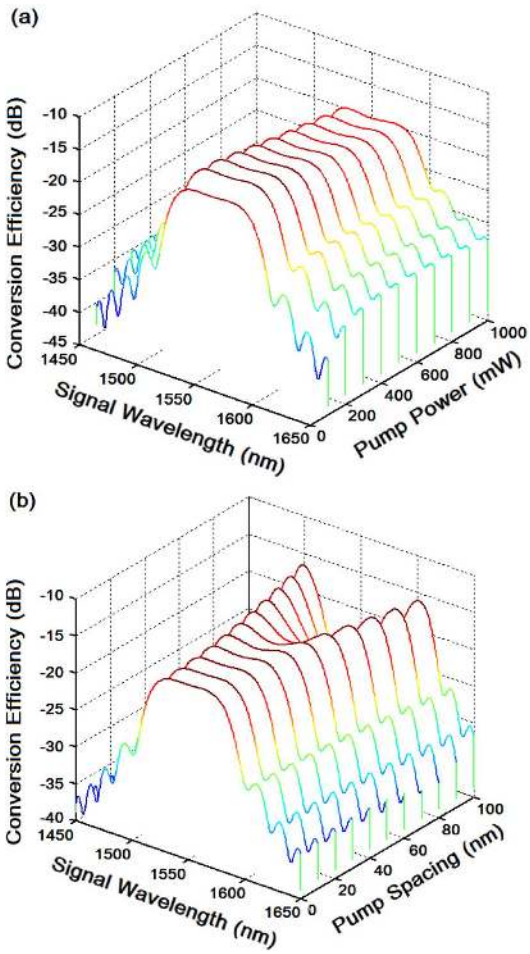

Fig. 7. Variation of the conversion response with (a) the pump power of the degenerate FWM or (b) the pump wavelength spacing of the nondegenerate FWM.

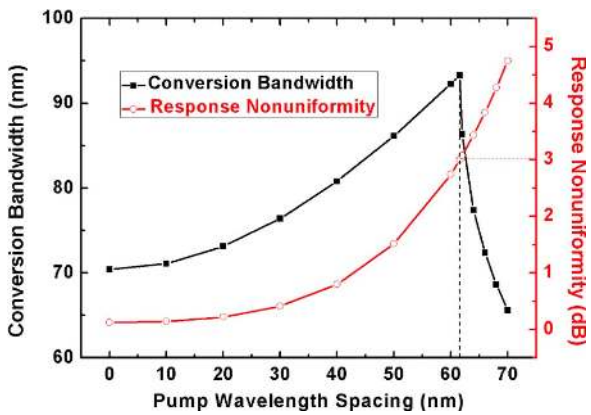

Fig. 8. Conversion bandwidth and the corresponding response nonuniformity as the pump wavelength spacing varies.

Therefore, it is reasonable to use the exact model shown in (1)–(4). Moreover, the free-carrier lifetime is a dominant factor of the FCA effect in the silicon waveguide. Here we simulate the influence of the free-carrier lifetime on the efficiency in Fig. 10, where both of the pump powers are 150 mW. It is shown that the efficiency is tightly related to the lifetime of the

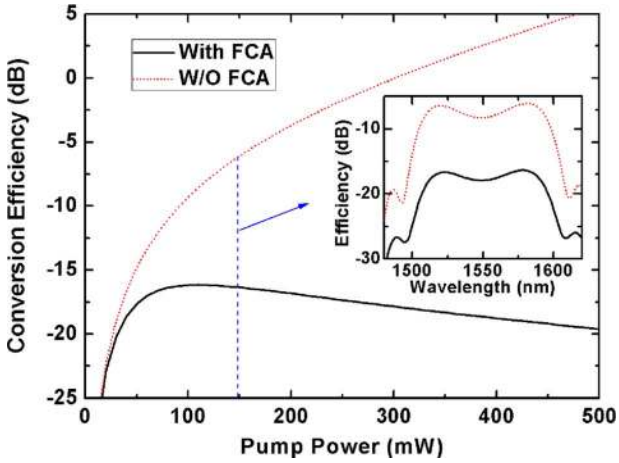

Fig. 9. Conversion efficiency comparison of the nondegenerate FWMs with and without FCA loss as the pump powers vary.

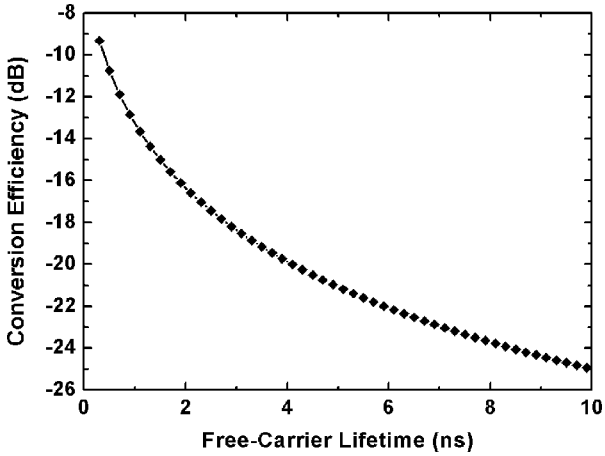

Fig. 10. Conversion efficiency of the nondegenerate FWM as the free-carrier lifetime in the silicon waveguide when the pump powers are adopted as 150 mW.

free carrier generated in the waveguide, which agrees well with the previous experimental contribution and the efficiency can be increased by shortening the free-carrier lifetime via reverse voltage [8].

In the following, we will compare the efficiency of the nondegenerate FWM with the degenerate FWM. According to the coupled equations (1)–(4), one can see that the conversion efficiency is dominated by two factors: the nonlinear loss due to TPA and FCA, and the phase-matching condition. For the nonlinear loss dominated by FCA, according to (9), the free-carrier density of the nondegenerate FWM can be simplified by ignoring the frequency difference between the TPA photons (i.e., $\nu = \nu_{p1} = \nu_{p2}$) and ignoring the contributions from weak signal and converted wave powers as

$$N = \frac{\beta_{\mathrm{TPA}}\tau}{2h\nu A_{\mathrm{eff}}^2}\left(P_{p1}^2 + P_{p2}^2 + 2P_{p1}P_{p2}\right) = \frac{\beta_{\mathrm{TPA}}\tau}{2h\nu A_{\mathrm{eff}}^2}(P_{P2} + P_{P2})^2. \tag{15}$$

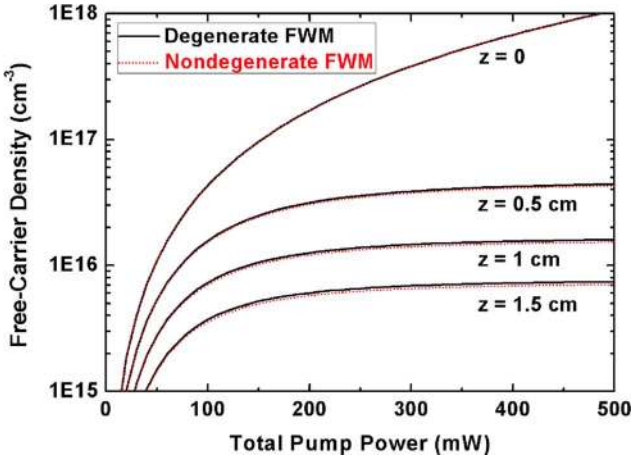

Fig. 11. Free-carrier densities of the nondegenerate and degenerate FWMs versus the total pump power for different positions in the silicon waveguide.

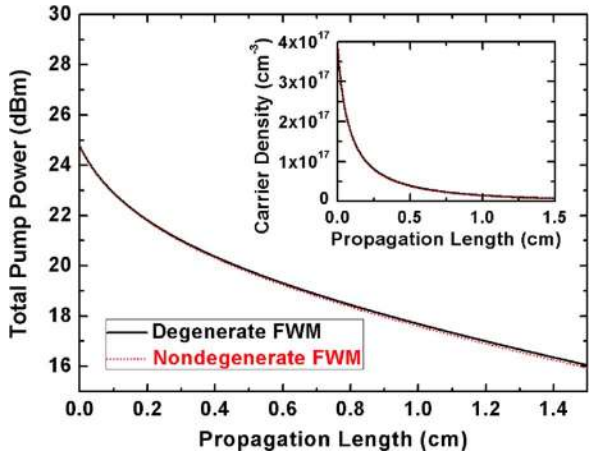

Fig. 12. Comparison of the total pump distribution for the nondegenerate and degenerate FWMs along the propagation length when the incident total pump power is 300 mW. The inset shows the carrier density comparison between the nondegenerate and degenerate FWMs.

Free carrier density for the degenerate FWM is calculated using a similar fashion [23] and we obtain

$$N' = \frac{\beta_{\mathrm{TPA}}\tau}{2h\nu A_{\mathrm{eff}}^2} P_p^2. \tag{16}$$

When the single-pump and two-pump FWMs have the same total pump power, that is, $P_{p1} + P_{p2} = P_p$, one can find that the free-carrier densities shown in (15) and (16) are also approximately the same, i.e., $N = N'$, which means the same FCA nonlinear loss. By further assuming $P_{p1} = P_{p2}$, the free-carrier densities of the nondegenerate and degenerate FWMs as the total pump power are calculated in Fig. 11, where several different positions in the above mentioned 300 nm $\times$ 650 nm silicon waveguide are considered and a free-carrier lifetime of 2 ns is used. In this simulation, we still use the exact expression of the FCA nonlinear-loss coefficient in (10). It is verified that the TPA-induced free-carrier densities are almost equal for the two kinds of FWMs, as predicted in (15) and (16). Fig. 12 shows the total pump power comparison between the nondegenerate and degenerate FWMs in the 1.5-cm-long waveguide. The two incident pump powers of the nondegenerate FWM are both assumed as 150 mW with a spacing of 50 nm and the pump power of the degenerate FWM is 300 mW. The inset shows the carrier densities along the waveguide for the two cases. One can see that the carrier density generated in the nondegenerate FWM is almost the same as that of the degenerate FWM and hence the distribution of the total pump power is also the same in the silicon waveguide.

On the other hand, the distributions of the phase-matching condition are quite different for the nondegenerate and degenerate FWMs even though their total pump powers are set to be the same, as analyzed in Section III. The signal near the pumps has a small phase mismatch both in degenerate FWM and in nondegenerate FWM. As a result, the conversion efficiency will be different for a fixed signal wavelength in the two regimes. As shown in Fig. 13(a), the 1550-nm signal, which is near the mean wavelength of the two pumps and far from each pump and hence suffers from large phase mismatch, has a lower conversion efficiency in the two-pump nondegenerate regime than

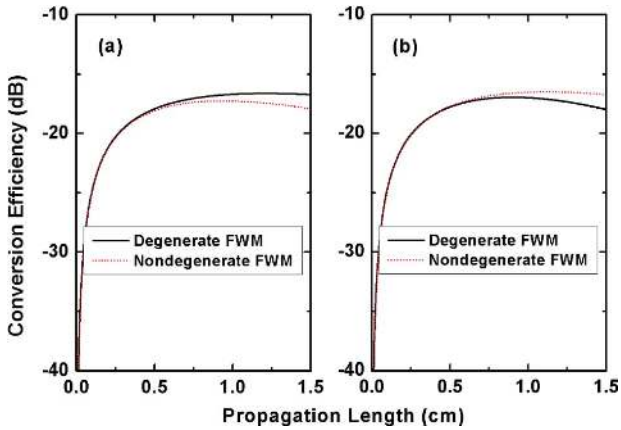

Fig. 13. Conversion efficiency comparison of the nondegenerate and degenerate FWMs corresponding to Fig. 12 for (a) the 1550-nm signal and (b) the 1585-nm signal.

in the single-pump regime since there it is very close to the pump and has a smaller phase mismatch. On the contrary, for the 1585-nm signal, which is near the phase-matching wavelengths of nondegenerate FWM and far from the phase-matching wavelength of degenerate FWM, the output nondegenerate efficiency is higher than the degenerate efficiency, as shown in Fig. 13(b).

We use the maximum efficiencies that can be obtained in the degenerate and nondegenerate FWMs to compare their efficiency performance. Fig. 14 shows the maximum conversion efficiency as the pump power increases, where the pump wavelength is 1550 nm for the degenerate FWM and the two pumps have a mean wavelength of 1550 nm and the pump spacing is optimized to achieve the maximum conversion bandwidth for the nondegenerate FWM. Here the two pump powers for the nondegenerate FWM are also considered to be the same. Simulation results show that the maximum efficiencies that can be achieved using nondegenerate and degenerate FWMs are almost the same. However, the required power of each pump (108 mW) to realize the maximum conversion efficiency in the nondegenerate FWM is much lower than that (216 mW) in the degenerate FWM although one more pump is needed. As we know,

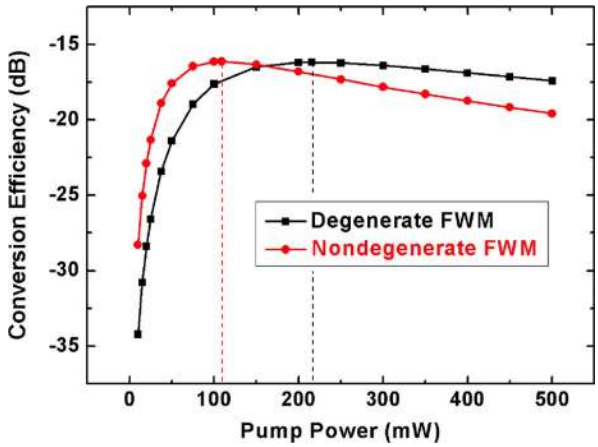

Fig. 14. Maximum conversion efficiencies of the nondegenerate and degenerate FWMs when the pump powers vary.

the incident pump power is still critical due to the power performance of laser diodes and the low coupling coefficient of silicon nanowire waveguides. The wavelength conversion based on two-pump nondegenerate FWM has more potential to realize the maximum conversion efficiency predicted by theoretical analysis.

V. Conclusion

The wavelength conversion based on nondegenerate FWM with two pumps has been investigated in a silicon nanowire waveguide. Analysis shows that the conversion bandwidth can be efficiently enhanced by separating the two pumps since the phase-matching condition can be easily tuned by the pump wavelengths. More than 30% bandwidth enhancement is numerically demonstrated in a 1.5-cm-long 300 nm $\times$ 650 nm silicon waveguide compared to the degenerate FWM with a single pump. The FCA losses in the nondegenerate and degenerate FWMs are almost the same and hence they have an approximately equal efficiency under the same total pump power condition regardless of the phase-matching condition. In practical applications, a high efficiency is easier to realize in the two-pump nondegenerate FWM regime since the required power is low for each pump. In this paper, we assumed that all involved waves in the FWM effect are co-polarized. If the waveguide birefringence is used, the free-carrier accumulation may be reduced [5] and the performance of wavelength conversion has the potential to be improved.

References

[1] Q. Lin, O. J. Painter, and G. P. Agrawal, "Nonlinear optical phenomena in silicon waveguides: Modeling and applications," *Opt. Exp.*, vol. 15, no. 25, pp. 16604–16644, Dec. 2007.

[2] I. D. Rukhlenko, M. Premaratne, and G. P. Agrawal, "Nonlinear silicon photonics: Analytical tools," *IEEE J. Sel. Top. Quantum Electron.*, vol. 16, no. 1, pp. 200–215, Jan.–Feb. 2010.

[3] R. Salem, M. A. Foster, A. C. Turner-Foster, D. F. Geraghty, M. Lipson, and A. L. Gaeta, "High-speed optical sampling using a silicon-chip temporal magnifier," *Opt. Exp.*, vol. 17, no. 6, pp. 4324–4329, Mar. 2009.

[4] M. A. Foster, A. C. Turner, J. E. Sharping, B. S. Schmidt, M. Lipson, and A. L. Gaeta, "Broad-band optical parametric gain on a silicon photonic chip," *Nature*, vol. 441, no. 7096, pp. 960–963, Jun. 2006.

[5] X. Sang and O. Boyraz, "Gain and noise characteristics of high-bit-rate silicon parametric amplifiers," *Opt. Exp.*, vol. 16, no. 17, pp. 13122–13132, Aug. 2008.

[6] R. Salem, M. A. Foster, A. C. Turner, D. F. Geraghty, M. Lipson, and A. L. Gaeta, "All-optical regeneration on a silicon chip," *Opt. Exp.*, vol. 15, no. 12, pp. 7802–7809, Jun. 2007.

[7] H. Fukuda, K. Yamada, T. Shoji, M. Takahashi, T. Tsuchizawa, T. Watanabe, J. Takahashi, and S. Itabashi, "Four-wave mixing in silicon wire waveguides," *Opt. Exp.*, vol. 13, no. 12, pp. 4629–4637, Jun. 2005.

[8] H. Rong, Y.-H. Kuo, A. Liu, M. Paniccia, and O. Cohen, "High efficiency wavelength conversion of 10 Gb/s data in silicon waveguides," *Opt. Exp.*, vol. 14, no. 3, pp. 1182–1188, Feb. 2006.

[9] K. Yamada, H. Fukuda, T. Tsuchizawa, T. Watanabe, T. Shoji, and S. Itabashi, "All-optical efficient wavelength conversion using silicon photonic wire waveguide," *IEEE Photon. Technol. Lett.*, vol. 18, no. 9, pp. 1046–1048, May 2006.

[10] B. G. Lee, A. Biberman, A. C. Turner-Foster, M. A. Foster, M. Lipson, A. L. Gaeta, and K. Bergman, "Demonstration of broadband wavelength conversion at 40 Gb/s in silicon waveguides," *IEEE Photon. Technol. Lett.*, vol. 21, no. 1–4, pp. 182–184, Jan.–Feb. 2009.

[11] R. L. Espinola, J. I. Dadap, R. M. Osgood, S. J. McNab, and Y. A. Vlasov, "C-band wavelength conversion in silicon photonic wire waveguides," *Opt. Exp.*, vol. 13, no. 11, pp. 4341–4349, May 2005.

[12] A. Melloni, F. Morichetti, and M. Martinelli, "Four-wave mixing and wavelength conversion in coupled-resonator optical waveguides," *J. Opt. Soc. Amer. B*, vol. 25, no. 12, pp. C87–C97, Dec. 2008.

[13] A. C. Turner, M. A. Foster, A. L. Gaeta, and M. Lipson, "Ultra-low power parametric frequency conversion in a silicon microring resonator," *Opt. Exp.*, vol. 16, no. 7, pp. 4881–4887, Mar. 2008.

[14] L. Jia, M. Geng, L. Zhang, L. Yang, P. Chen, Y. Liu, Q. Fang, and M. Yu, "Effects of waveguide length and pump power on the efficiency of wavelength conversion in silicon nanowire waveguides," *Opt. Lett.*, vol. 34, no. 22, pp. 3502–3504, Nov. 2009.

[15] Q. Lin, J. Zhang, P. M. Fauchet, and G. P. Agrawal, "Ultrabroadband parametric generation and wavelength conversion in silicon waveguides," *Opt. Exp.*, vol. 14, no. 11, pp. 4786–4799, May 2006.

[16] X. Zhang, S. Gao, and S. He, "Optimal design of a silicon-on-insulator nanowire waveguide for broadband wavelength conversion," *Prog. Electromagn. Res.*, vol. 89, pp. 183–198, Jan. 2009.

[17] X. Liu, W. M. J. Green, X. Chen, I.-W. Hsieh, J. I. Dadap, Y. A. Vlasov, and R. M. Osgood, Jr., "Conformal dielectric overlayers for engineering dispersion and effective nonlinearity of silicon nanophotonic wires," *Opt. Lett.*, vol. 33, no. 24, pp. 2889–2891, Dec. 2008.

[18] S. Gao, X. Zhang, Z. Li, and S. He, "Polarization-independent wavelength conversion using an angled-polarization pump in a silicon nanowire waveguide," *IEEE J. Sel. Top. Quantum Electron.*, vol. 16, no. 1, pp. 250–256, Jan.–Feb. 2010.

[19] S. Gao, E.-K. Tien, Q. Song, Y. Huang, and O. Boyraz, "Ultra-broadband one-to-two wavelength conversion using low-phase-mismatching four-wave mixing in silicon waveguides," *Opt. Exp.*, vol. 18, no. 11, pp. 11898–11903, May 2010.

[20] J. S. Park, S. Zlatanovic, M. L. Cooper, J. M. Chavez-Boggio, I. B. Divliansky, N. Alic, S. Mookherjea, and S. Radic, "Two-pump four-wave mixing in silicon waveguides," in *Proc. Frontiers in Optics, OSA Tech. Dig.*, San Jose, CA, 2009, paper FML2.

[21] D. C. Hutchings and E. W. Van Stryland, "Nondegenerate two-photon absorption in zinc blende semiconductors," *J. Opt. Soc. Amer. B*, vol. 9, no. 11, pp. 2065–2074, Nov. 1992.

[22] T. K. Liang and H. K. Tsang, "Role of free carriers from two-photon absorption in Raman amplification in silicon-on-insulator waveguides," *Appl. Phys. Lett.*, vol. 84, no. 15, pp. 2745–2747, Apr. 2004.

[23] A. Liu, H. Rong, R. Jones, O. Cohen, D. Hak, and M. Paniccia, "Optical amplification and lasing by stimulated Raman scattering in silicon waveguides," *J. Lightw. Technol.*, vol. 24, no. 3, pp. 1440–1455, Mar. 2006.

[24] M. A. Foster, A. C. Turner, R. Salem, M. Lipson, and A. L. Gaeta, "Broad-band continuous-wave parametric wavelength conversion in silicon nanowaveguides," *Opt. Exp.*, vol. 15, no. 20, pp. 12949–12958, Oct. 2007.

[25] S. Gao, Z. Li, and X. Zhang, "Power-attenuated optimization for four-wave mixing-based wavelength conversion in silicon nanowire waveguides," *J. Electromagn. Waves Appl.*, vol. 24, no. 8–9, pp. 1255–1265, 2010.

Author biographies not included at authors' request due to space constraints.